

Supplementary Information

A single isomer rotary switch demonstrating anti-Kasha behavior: Does acidity function matter?

Anton Georgiev^{a,b}, Dancho Yordanov^{c,d}, Nikolay Vassilev^{c,d}, Vera Deneva^{c,d}, Daniela Nedeltcheva^{c,d}, Ivan Angelov^d and Liudmil Antonov^d

^a *Department of Organic Chemistry, University of Chemical Technology and Metallurgy, 1756 Sofia, Bulgaria*

^b *Institute of Optical Materials and Technologies, Bulgarian Academy of Sciences, 1113 Sofia, Bulgaria*

^c *Institute of Organic Chemistry with Centre of Phytochemistry, Bulgarian Academy of Sciences, 1113 Sofia, Bulgaria*

^d *Institute of Electronics, Bulgarian Academy of Sciences, 1784 Sofia, Bulgaria*

Content:

Structural elucidation of 2 (Figs. S1 and S2)	2
¹ H NMR spectrum of 1 (Fig. S3)	3
¹³ C NMR spectra of 1 and 2 (Fig. S4)	4
Additional structure elucidation the most stable isomer of 2 (Scheme S1, Figs. S5-S7)	5
Irradiation experiments (Figs. S8-S10)	9
Ground state energy landscape (Scheme S2)	12
Frontier molecular orbitals of 1 and 2 (Table S1)	13
Absorption and emission spectra of 1 (Fig. S11)	17
Time dependent experiments of 2 (Figs. S12-S13)	18
A Absorption and emission spectra of 2 in CH ₂ Cl ₂ (Fig. S14)	24
Protonation experiments and calculations of 2 (Table S2, Figs. S15-S16)	25
References	26

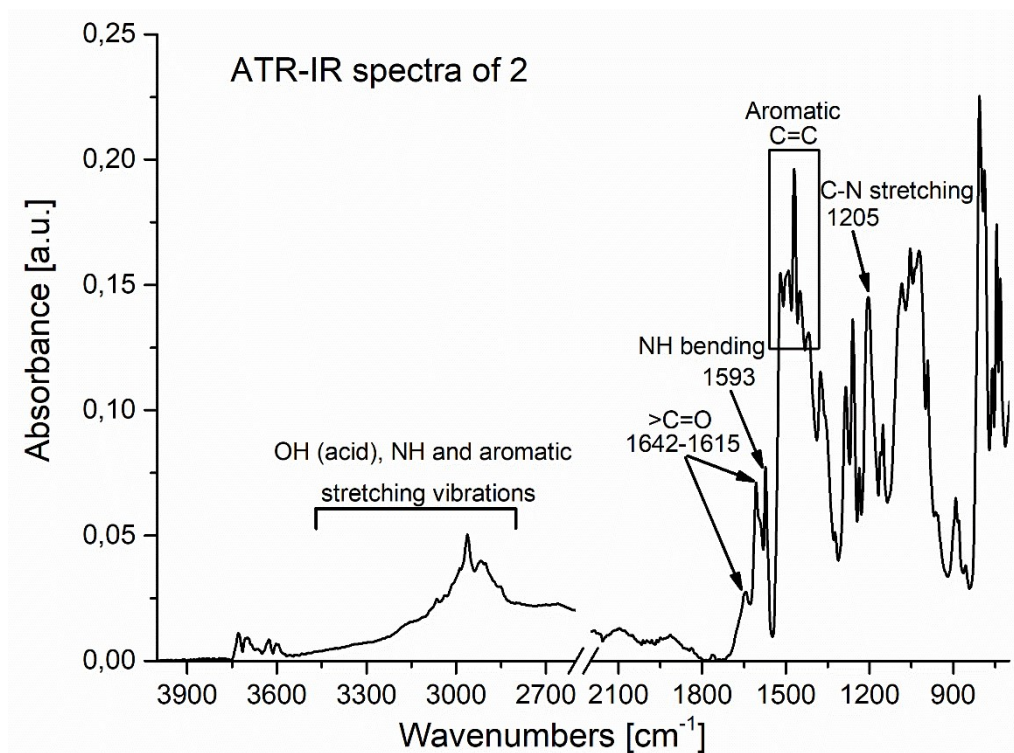


Fig. S1. ATR-IR spectrum of 2.

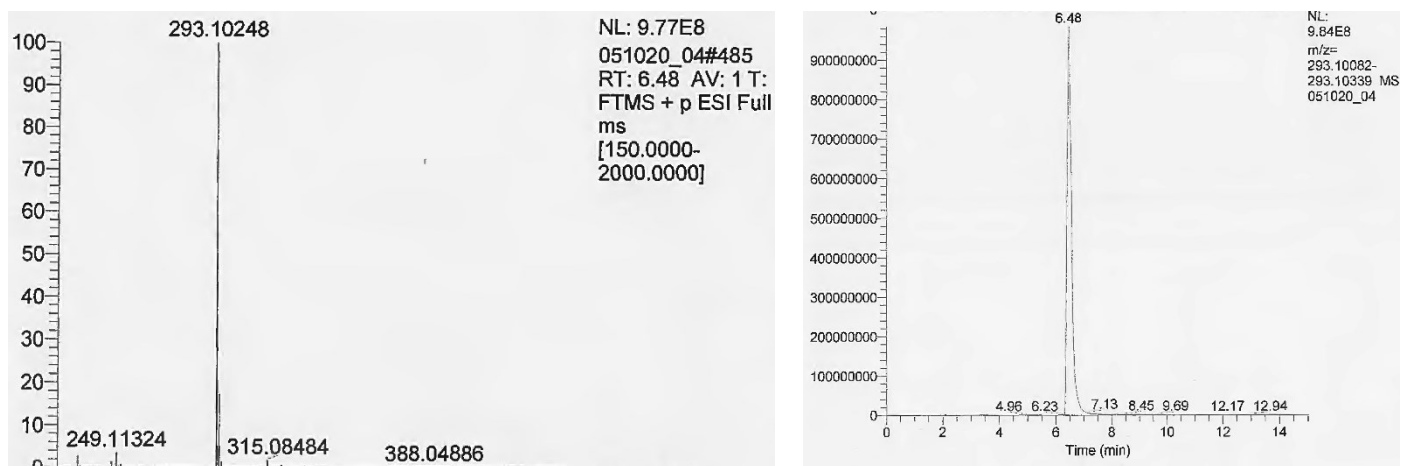


Fig. S2. HRMS of 2: exact mass M+1 (left) and chromatogram (right)

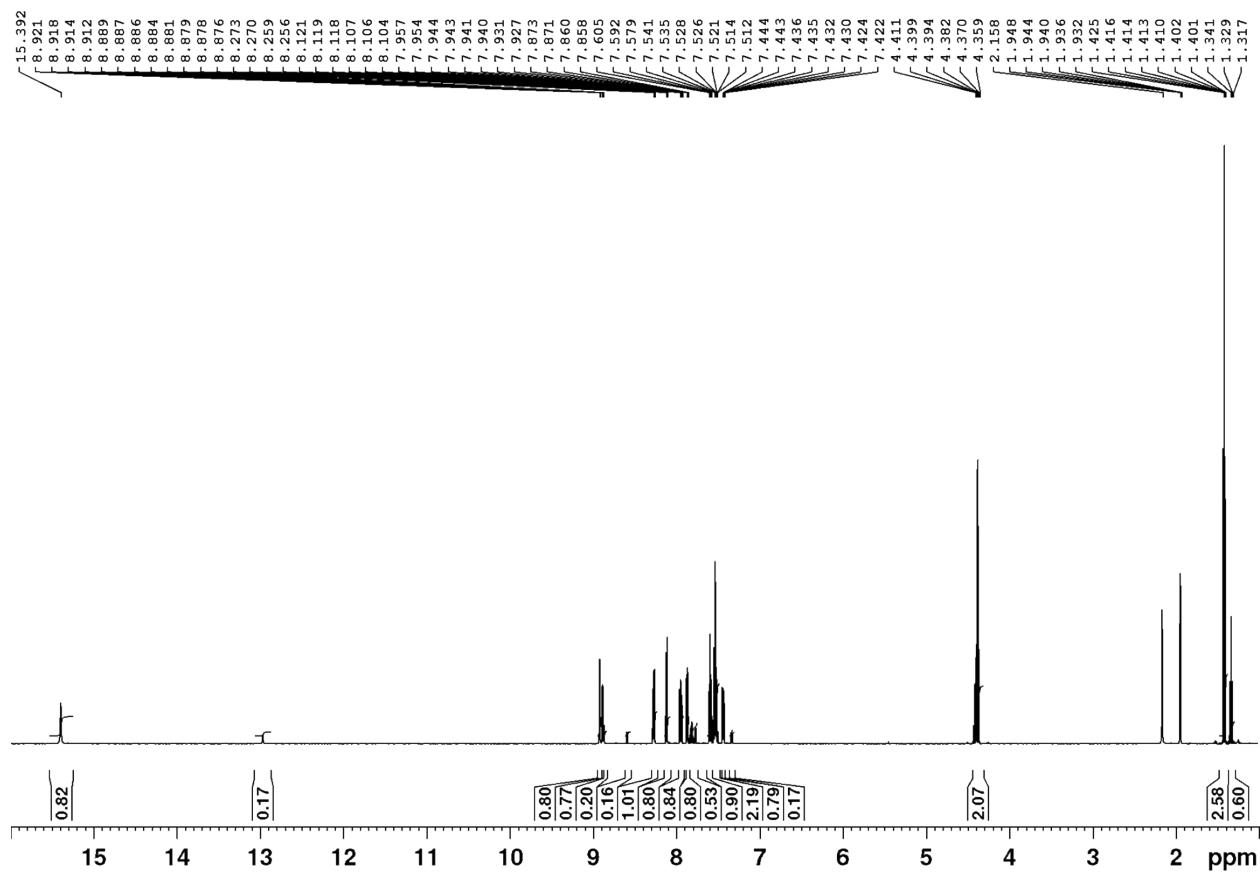


Fig. S3. $^1\text{H-NMR}$ spectrum of **1** in CD_3CN .

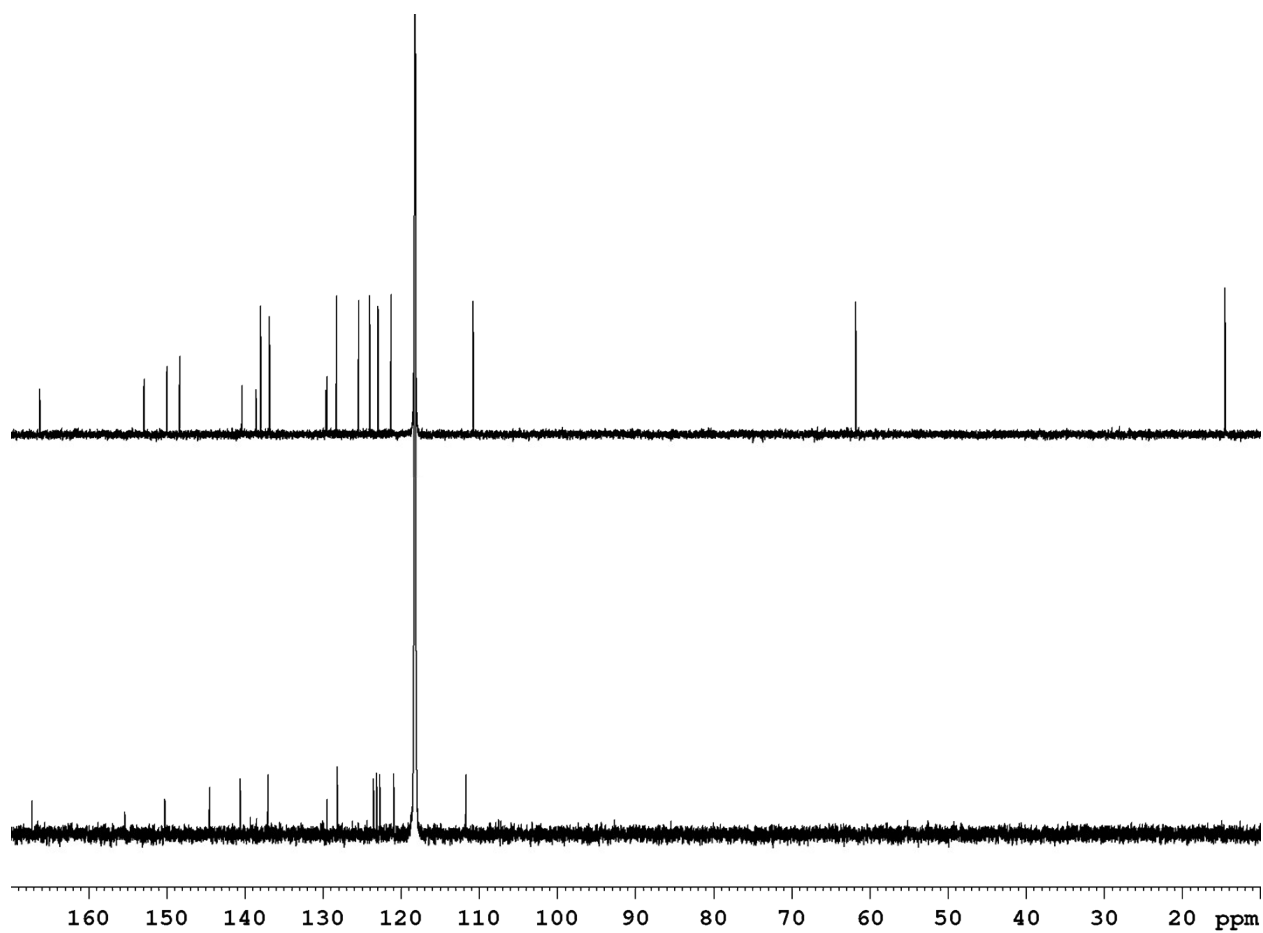
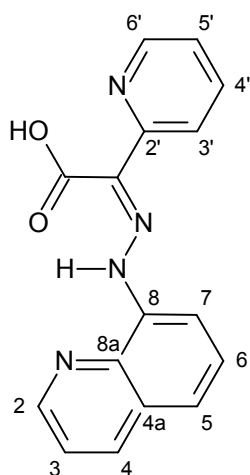


Fig. S4. ^{13}C -NMR spectra of **1** (top) and **2** (bottom) in CD_3CN .

Additional structure elucidation the most stable isomer of compound **2**:

In order to assign the proton and carbon shifts of NMR spectra of compound **2** in CDCl_3 , CD_3CN and $\text{DMSO-}d_6$, ^1H , ^{13}C , DEPT, 2D COSY, 2D NOESY, 2D HSQC and 2D HMBC spectra were measured. Figs. S5-S7 show 2D COSY, 2D HSQC and 2D NOESY spectra of compound **2** in CD_3CN with signal designation. In addition to 2D NOESY several 1D NOESY experiments were performed (not shown) in order to determine the conformation of compound **2**. The 1D NOESY spectra does not provide additional information comparing to 2D NOESY spectra. The registered NOE effects are only between the protons in the same aromatic system. This result could support the conclusion that the two aromatic systems are far from each other and is consistent with the conclusion that the conformation of compound **2** is Z.



Scheme S1. Atom numbering in **2**.

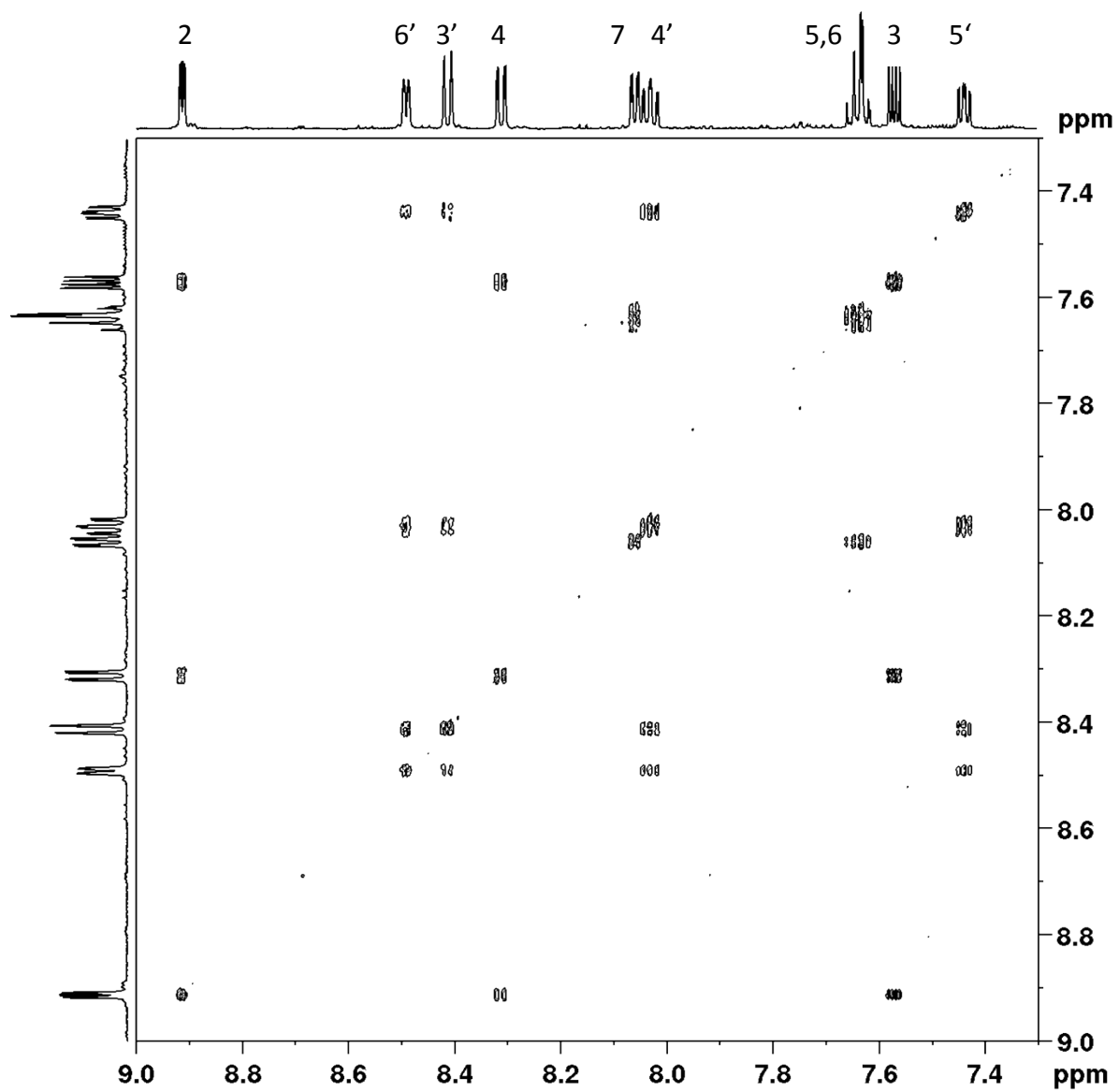


Fig. S5. 2D COSY spectrum of **2** in CD₃CN (see Scheme S1 for atom numbering).

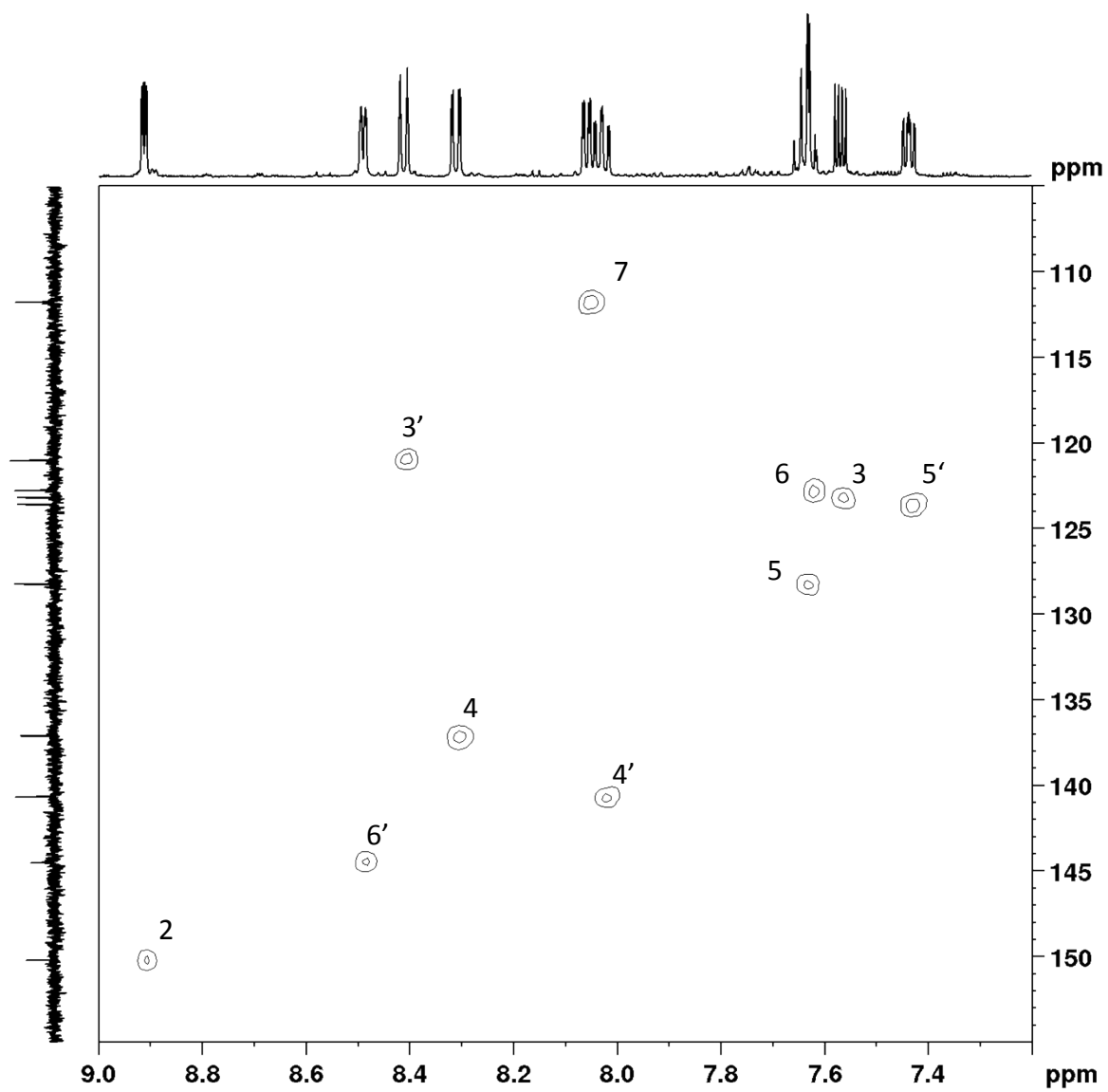


Fig. S6. 2D HSQC spectrum of **2** in CD_3CN (see Scheme S1 for atom numbering).

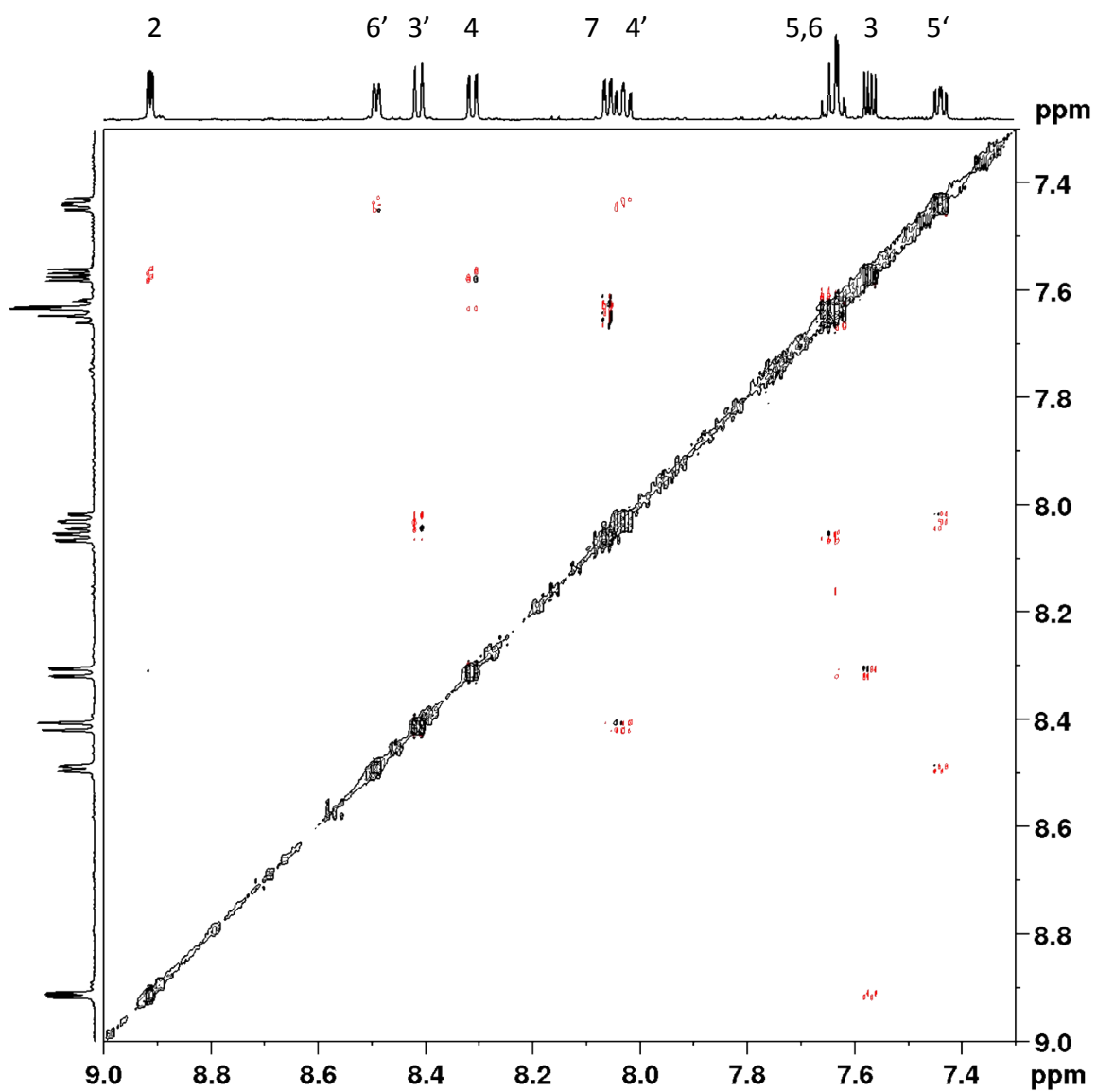


Fig. S7. 2D NOESY spectrum of **2** in CD₃CN (see Scheme S1 for atom numbering).

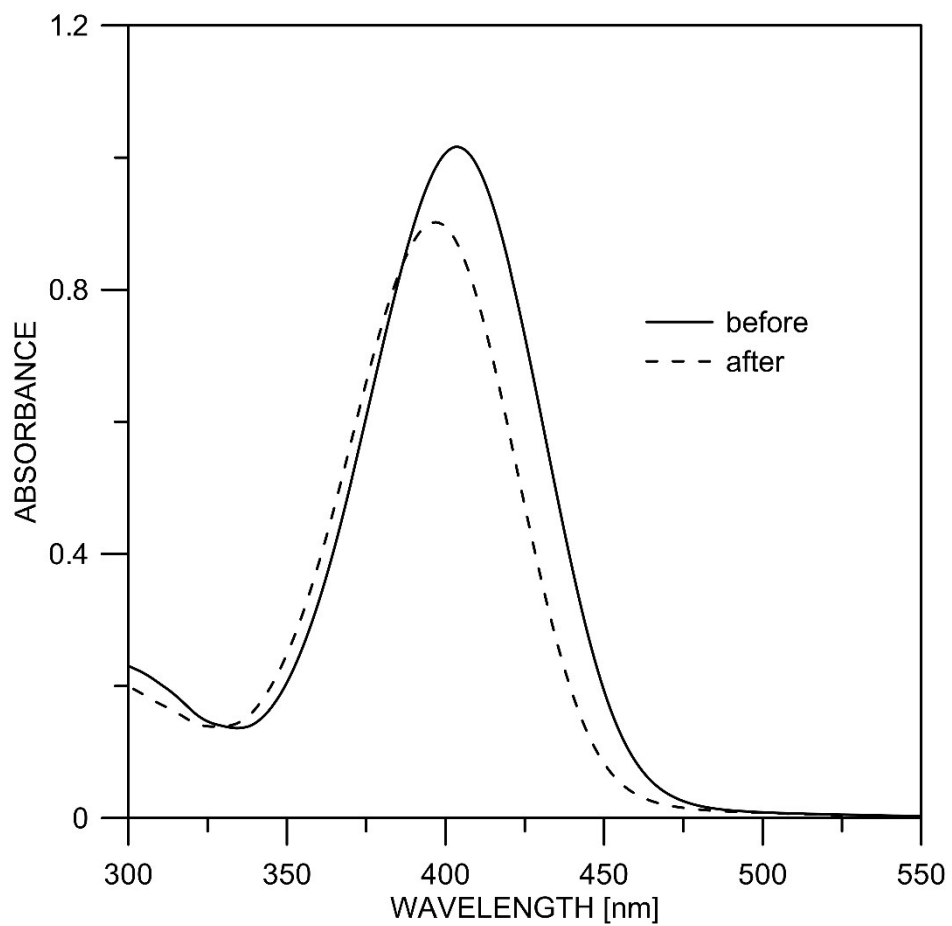


Fig. S8. The spectra of **2** in acetonitrile before and after irradiation at 405 nm.

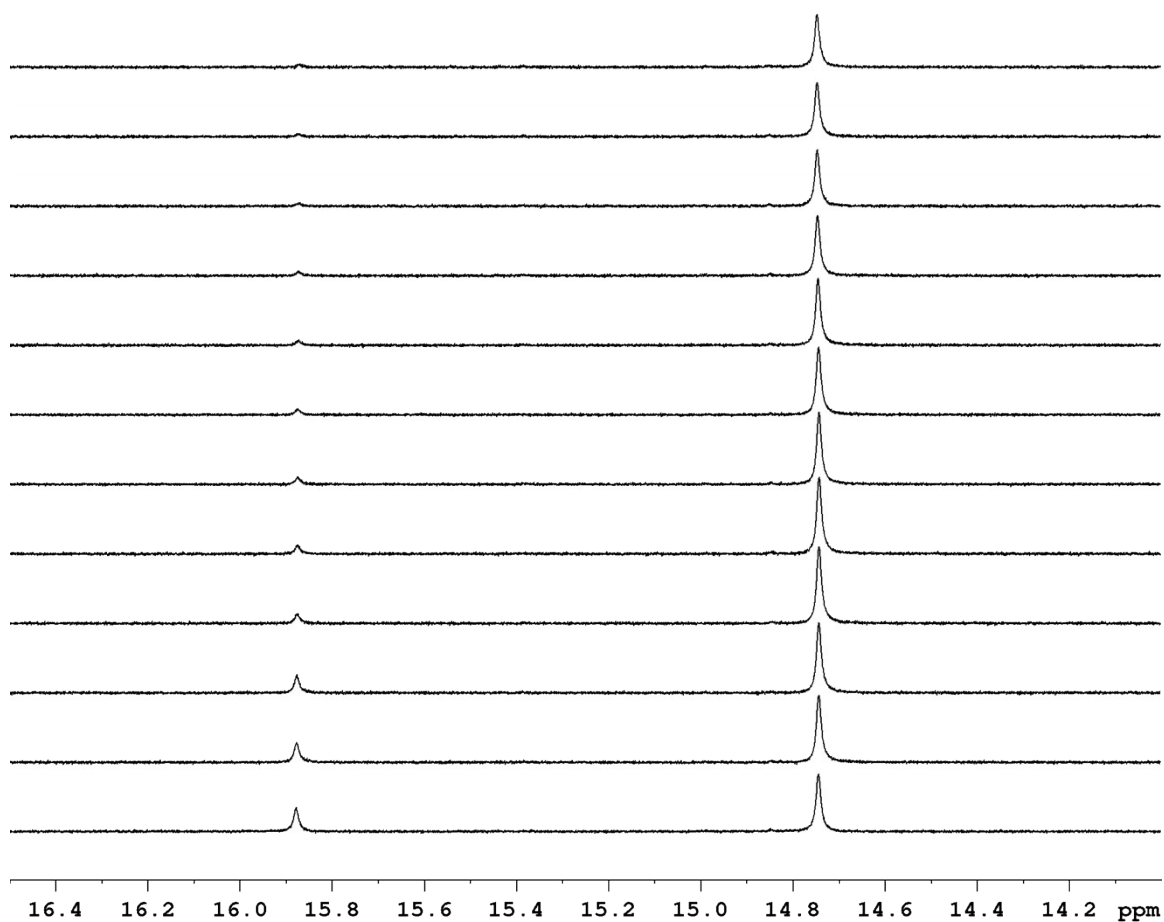


Fig. S9. ¹H NMR of **2** in CD₃CN after irradiation at 405 nm; spectra measured at (from down to up) 5 min, 10 min, 2 h, 3 h, 8 h, 9.5 h, 10 h, 12 h, 14 h, 16 h, 18 h, 19 h and 20 h after the stop of the irradiation.

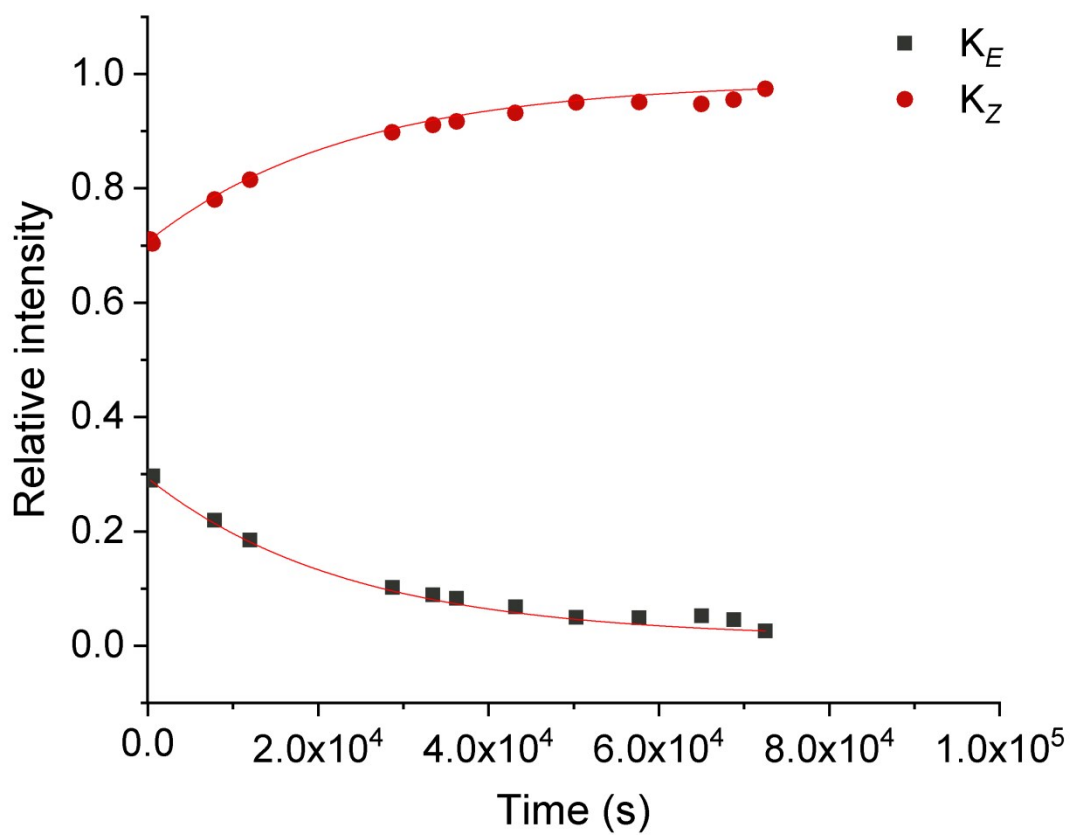
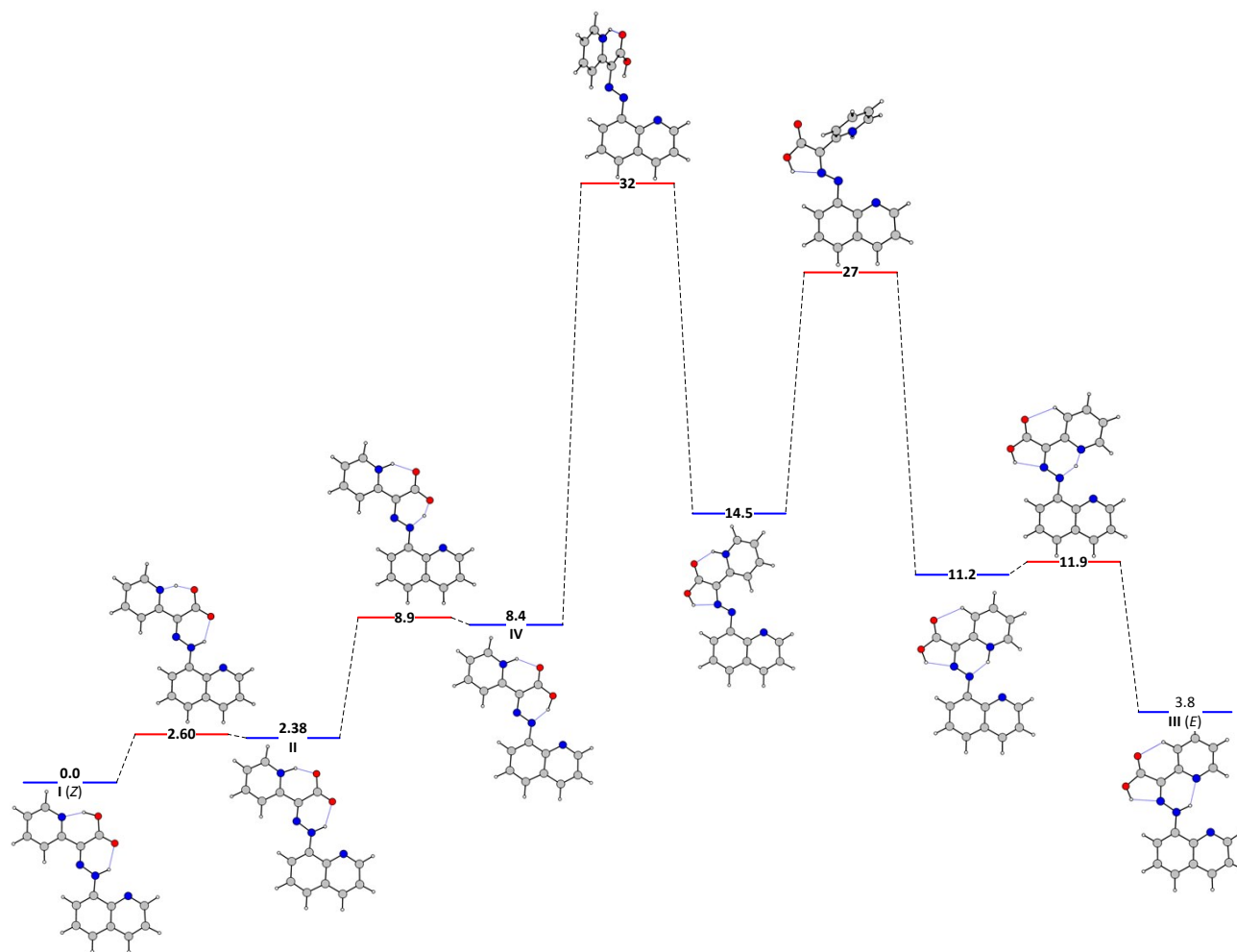


Fig. S10. Change of the relative NMR signals of **2** with the time, relaxation of *E* (black) and *Z* (red) in ACN after irradiation at 400 nm.



Scheme S2. Ground state energy landscape of 2 in ACN (M06-2X/TZVP, PCM solvent model). The values are given in kcal/mol units. The numbering of the structures is the same as in Table 1.

Table S1. Frontier molecular orbitals of **1E**, **1Z** and **2Z**.

Orbital	1E	1Z	2Z
HOMO-2			
HOMO-1			
HOMO			
LUMO			

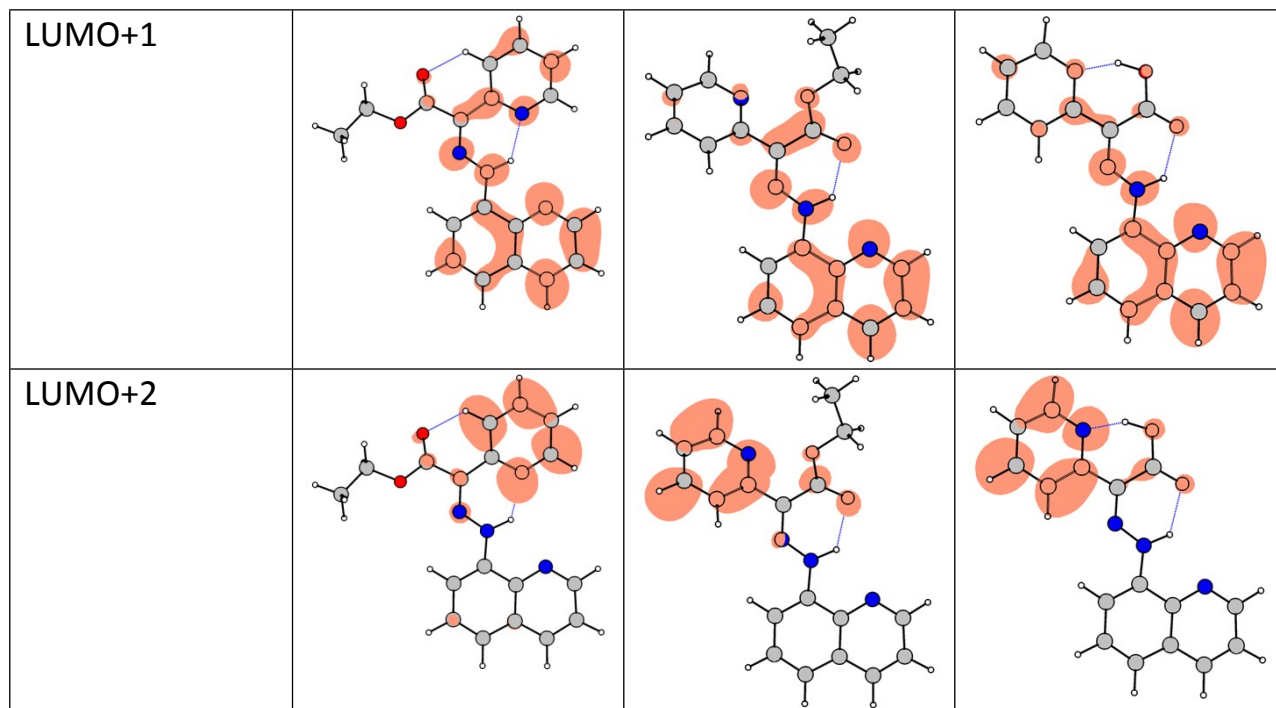
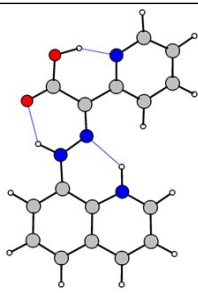
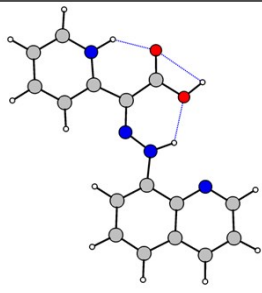
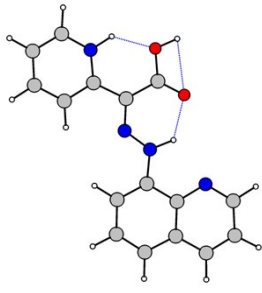
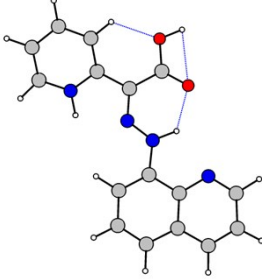
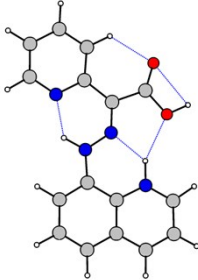
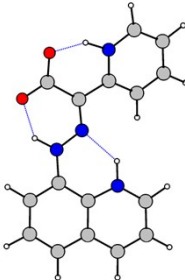


Table S2. Relative stability (M06-2X/TZVP) of the most stable protonated conformers and isomers of **2** in ACN.

Structure	ΔE (ΔG) [kcal mol ⁻¹]	UV-Vis (B3LYP/TZVP// M06-2X/TZVP)		¹ H NMR [ppm]		
		λ_{\max} [nm]	f			
 <p>V</p>	0.0 (0.0)	459	0.220	18.47 OH	14.12 NH	15.75 N _{quin} H
 <p>VI</p>	0.56 (0.04)	419	0.773	8.28 OH	13.86 NH	15.02 N _{pyr} H
 <p>VII</p>	0.97 (0.14)	420	0.760	7.93 OH	15.0 NH	13.70 N _{pyr} H

 <p style="text-align: center;">VIII</p>	<p style="text-align: center;">1.23 (1.49)</p>	<p style="text-align: center;">441</p>	<p style="text-align: center;">0.616</p>	<p style="text-align: center;">7.71 OH</p>	<p style="text-align: center;">14.98 NH</p>	<p style="text-align: center;">12.51 N_{pyr}H</p>
 <p style="text-align: center;">IX</p>	<p style="text-align: center;">1.71 (1.87)</p>	<p style="text-align: center;">459</p>	<p style="text-align: center;">0.234</p>	<p style="text-align: center;">7.23 OH</p>	<p style="text-align: center;">16.13 NH</p>	<p style="text-align: center;">17.01 N_{quin}H</p>
 <p style="text-align: center;">X</p>	<p style="text-align: center;">1.91 (1.63)</p>	<p style="text-align: center;">466</p>	<p style="text-align: center;">0.247</p>	<p style="text-align: center;">15.64 N_{quin}H</p>	<p style="text-align: center;">15.82 NH</p>	<p style="text-align: center;">20.27 N_{pyr}H</p>

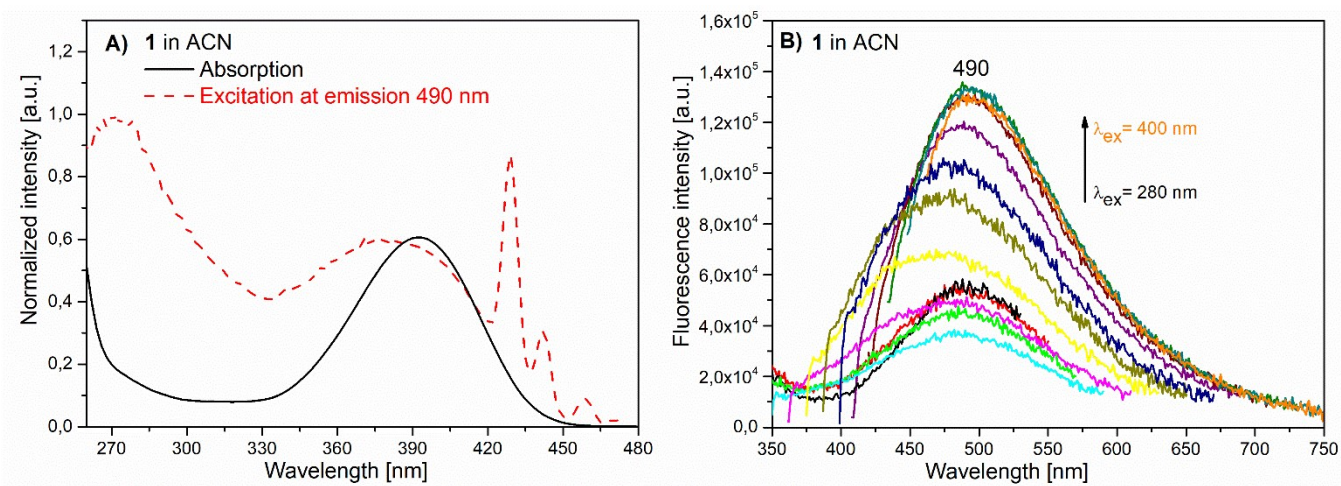


Fig. S11. Spectra of **1** in ACN: **A)** absorption and excitation spectra of **1**; **B)** excitation-dependent emission of **1** by $\lambda_{ex} = 280 \div 400$ nm.

Additional details related to the anti-Kasha ESIPT behavior:

According to the Kasha's rule, fluorescence can occur from the lowest excited energy level S_1 ¹. The opposite process - the absorption of light - can occur as a transition to any excited state. Since only one energy level is involved in the fluorescence process, this rule means that the shape of the fluorescence spectrum² as well as the fluorescence lifetime do not depend on the wavelength of the exciting light. Thus, in the case of a condensed phase fluorescence emitting only the $S_1 \rightarrow S_0$ transition and phosphorescence emitting only for transition $T_1 \rightarrow S_0$ can be observed, which means that the wavelength of the emitted light will always be greater than that of the excitation light.

This rule has no theoretical justification and simply reflects the fact that the speed of nonradiative transitions from high energy levels ($S_2, S_3 \dots (S^*), T_2, T_3 \dots (T^*)$) to the lowest vibrational sublevel of states S_1 or T_1 is so high compared to the rate of radiative transitions from these upper states, that the radiation appears only from the lower vibrational sublevel of the electronic energy levels S_1 or T_1 .

One of the most commonly used methods for retrieving information in studying the interactions of substances is to study the lifetime of the excited state of a known fluorophore and how it is affected by the presence of other compounds in the test medium³. Relatively little attention is paid to the process of population growth of the excited state from which we observe fluorescence and the information that can be extracted from this process. This is because the processes involved are extremely fast and difficult to distinguish as a contribution to the population level of the S_1 excited state. If the absorption of light is in the range of femtoseconds (10^{-15} s) and the known speeds of relaxation processes - internal conversion (10^{-12} - 10^{-9} s), vibrational relaxation (10^{-14} - 10^{-11} s) and intersystem crossing (10^{-11} - 10^{-8} s), their possible sequence in depending on the quantum-mechanical rules, would ultimately give us information about the delay times targeting to the population of the energy level from which the fluorescent signal is observed.

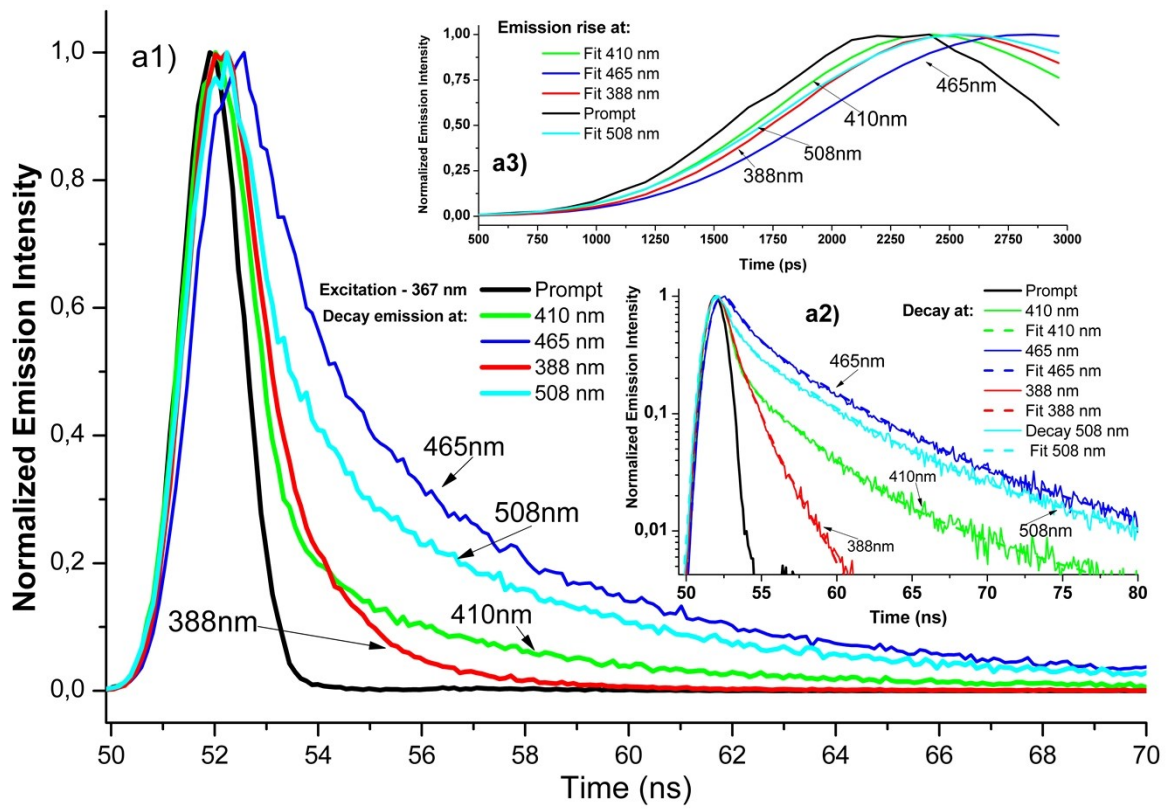
The normalized decay curves of the fluorescence intensity at 388, 410, 465 and 508 nm (367 nm excitation) and 420, 465 and 508 nm (405 nm excitation) are shown on Figs. 4 and S12. The deconvolution procedure leading to the best χ^2 criteria, shows that the three-exponential fitting leads to the best results for all emission decay curves obtained at excitation wavelengths 367 and 405 nm. The comparison of the values for obtained decay lifetimes lead to conclusion that decay of excited states can be approximated with fast and slow components, respectively, in the pico- and nanosecond time ranges (Fig. S13).

It should also be noted that the decay curves for the three fluorescence lengths examined at excitation 405 nm have the same behavior (comparing Figs. 4 and S12). When the compound is excited at 367 nm, as seen in Fig. 4, the decay behavior at 388 nm is different from the other decay curves. This is also found in the analysis of the values of the times, characteristic the decay of the excited states (Fig. S13a). It can be noted that the difference in the "slow" processes (respectively, the values for T1 and T3 in the used three exponential fitting of the processes) for the emissions of 410, 420, 465 and 508 nm are not significant, while at the values for the "fast" component (T2) we have almost one order of magnitude difference in values for the observed fluorescent wavelengths.

Analyzing the difference in the nature of the decay of the excited state with emissions at 388nm, we can note the following.

First, the emission of 388 nm in its predominant part (it is estimated that more than 70% of the accumulated photons in this energy state) was realized before the time of reaching the maximum emission of a wavelength of 465 nm (ESIPT transition S_n-S_0). This is a confirmation of the possibility to observe fluorescent radiation which does not fall within the scope of Kasha's rule.

Second, the difference in the T2 values in this case shows for another, perhaps non-equilibrium nature of the decay process, most probably due a competitive process in the excited state, such as a proton transfer for example. In confirmation of this it can be pointed out, as can be seen from Fig. 12a(a3), differences in growth rate and time to obtain maximum emission at 410 nm. The time to reach the maximum is about 20 ps less than this at 388nm. As can be seen from Figs. 4 and S13a the decay parameter T2 for 410 nm after reaching the fluorescent maximum is slower than at 388 nm, and at later stages the decay has the character as that at 465 nm. This can be explained by the assumption that the emission of this wavelength occurs as a result of the transition $ST^* - ST_0$, where by ST is meant the energy states of the tautomer. This is possible because in a higher excited states (S^*) the ESIPT process, due to very fast transition S^*-ST^* , with a typical transition time in a interval from a femto- up to a few picoseconds², conditions can be achieved to observe the fluorescence of this transition.



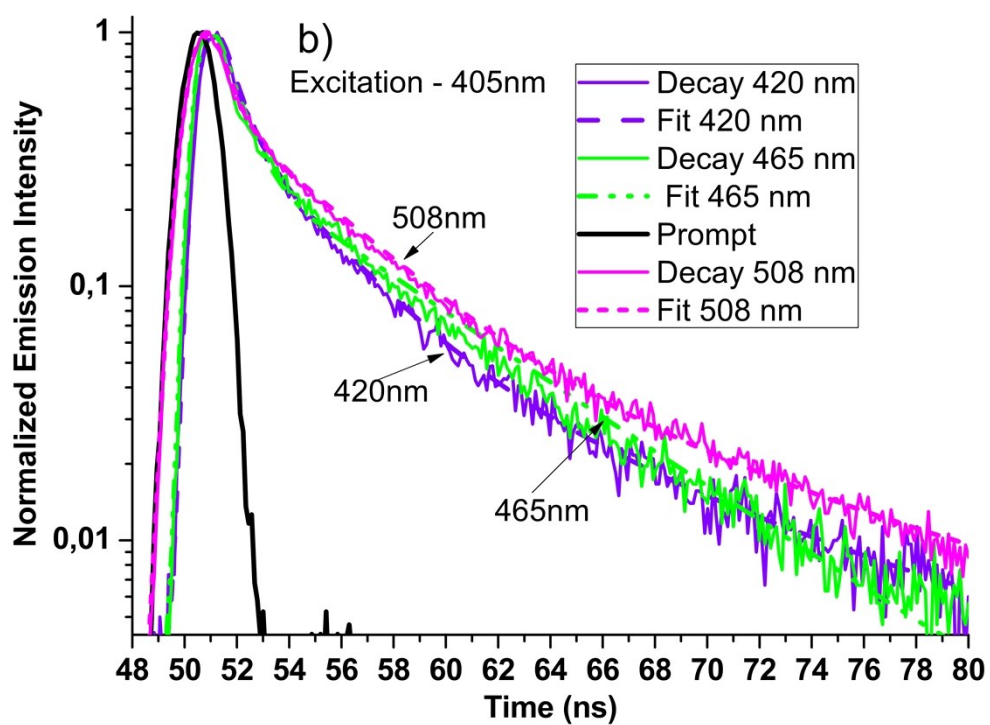
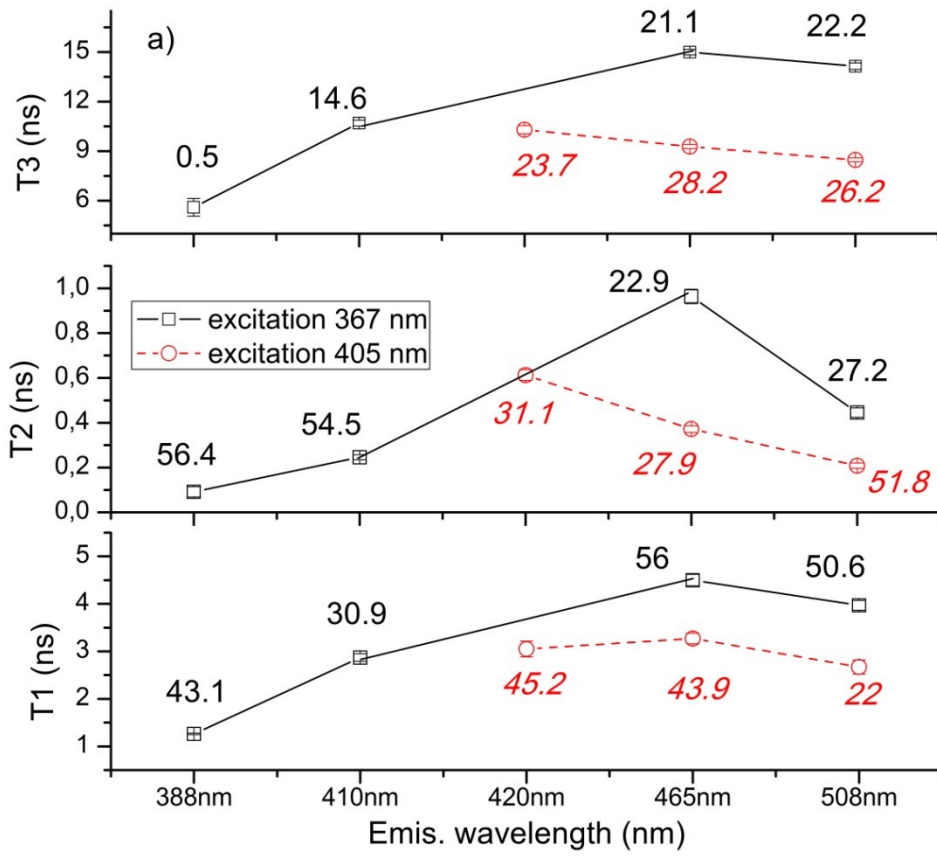


Fig. S12. The normalized kinetics for the excited state lifetimes of **1**, excited at 367 (a) and 405 (b) nm.



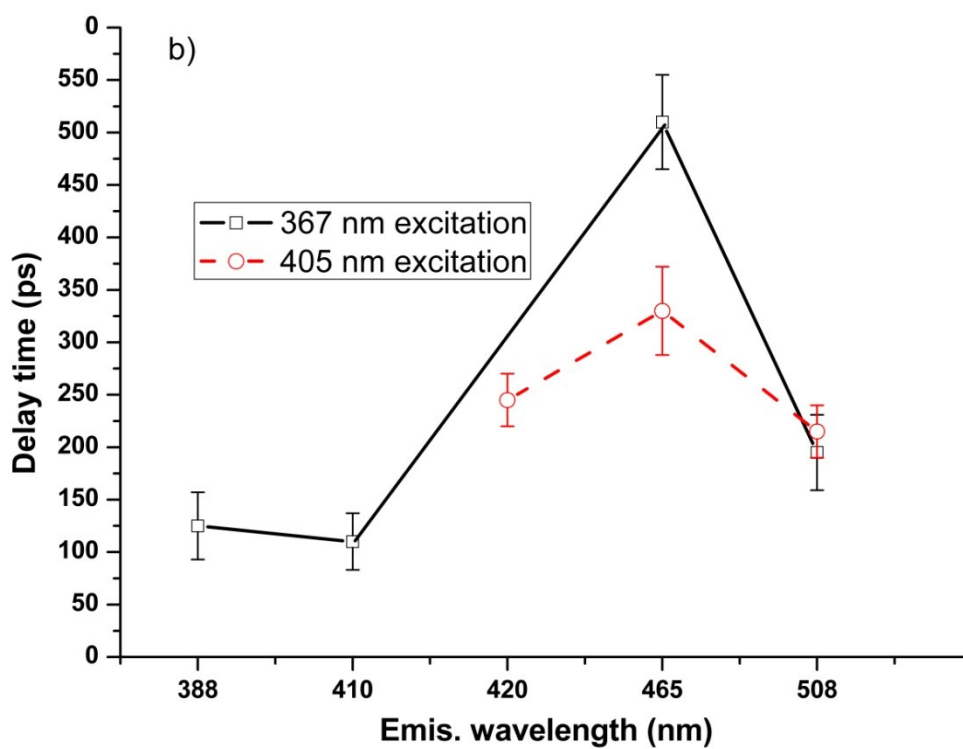


Fig. S13. The values (T_1 , T_2 and T_3) for the decay times and the corresponding pre-exponential factors obtained by fitting with three exponential functions (a) and measured delay times of the fluorescence maximum compared to the maximum of the excitation light pulses for the studied emission wavelengths (b) at excitation at 377 and 405 nm.

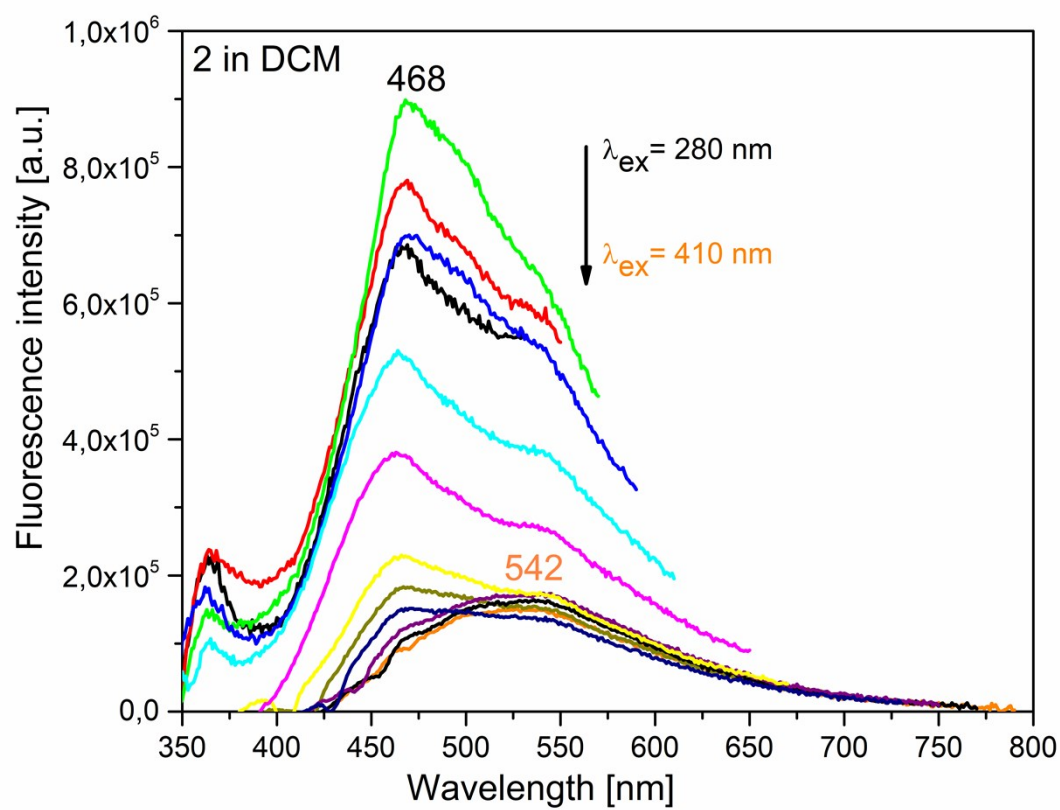


Fig. S14. Excitation-dependent emission of **2** in CH_2Cl_2 , obtained by stepwise (by 10 nm) change of λ_{ex} from 280 (in back) to 410 (in orange) nm.

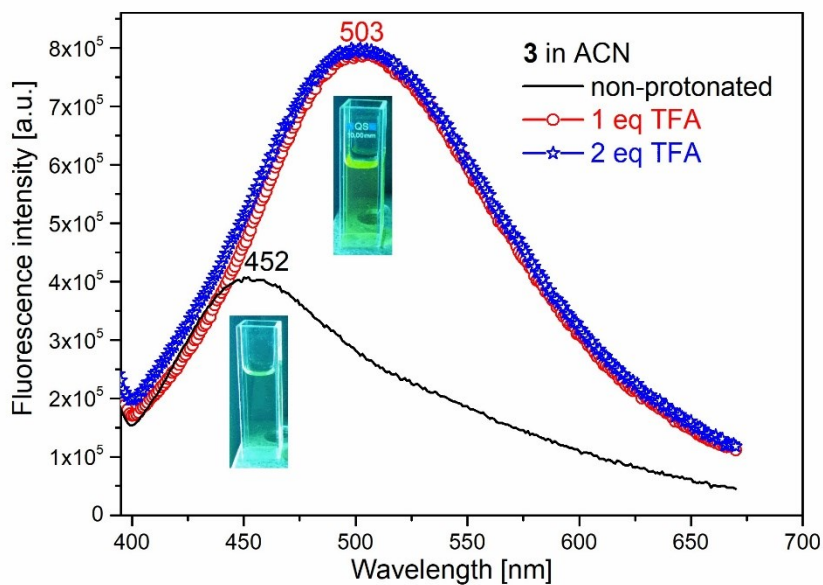


Fig. S15. Emissions of **2** in ACN, non-protonated and protonated forms with 1 and 2 eq TFA with excitation wavelength at 360 nm.

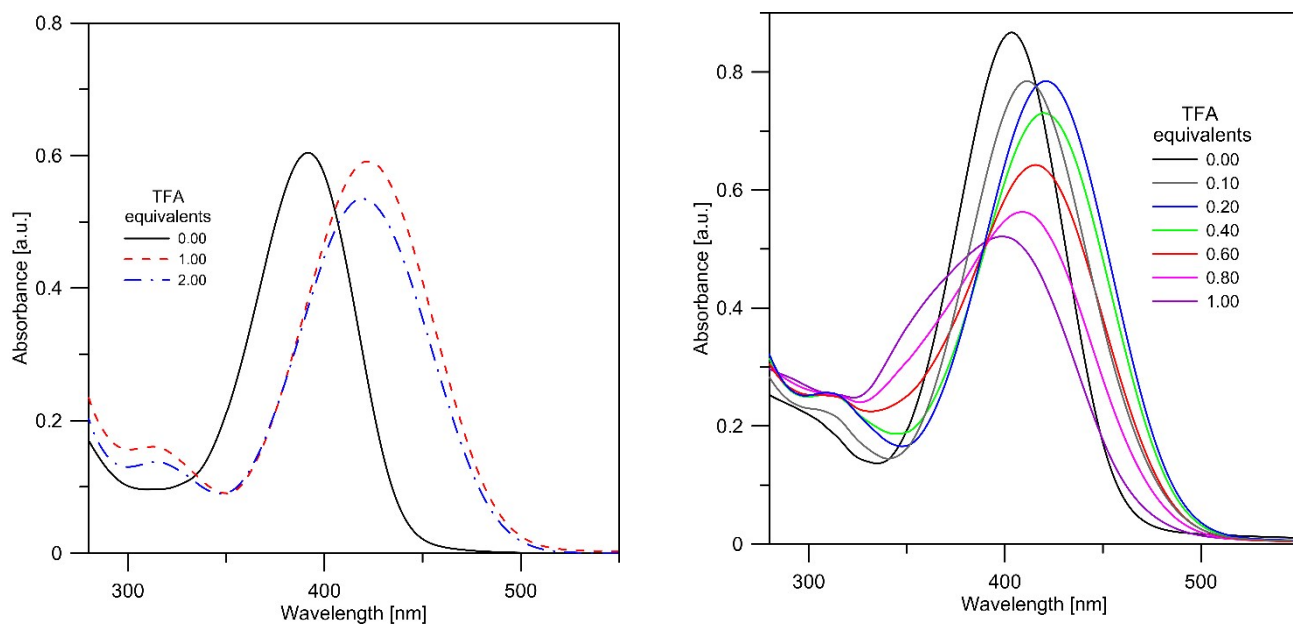


Fig. S16. Absorption spectra of **1** (left) and **2** (right) in ACN upon protonation with TFA.

References:

- 1 M. Kasha and S. P. McGlynn, *Annu. Rev. Phys. Chem.*, 1956, **7**, 403–424.
- 2 A. P. Demchenko, V. I. Tomin and P.-T. Chou, *Chem. Rev.*, 2017, **117**, 13353–13381.
- 3 J. R. Lakowicz, *Principles of fluorescence spectroscopy*, Springer, New York, NY, Third edition, corrected at 4. printing., 2010.